# Fuel Composition and Diluent Effect on Gas Transport and Performance of Anode-Supported SOFCs

*Journal of The Electrochemical Society*, **150** (7) A942-A951 (2003)
0013-4651/2003/150(7)/A942/10/$7.00 © The Electrochemical Society, Inc.

# Fuel Composition and Diluent Effect on Gas Transport and Performance of Anode-Supported SOFCs

**Yi Jiang* and Anil V. Virkar*,z**

*Department of Materials Science and Engineering, University of Utah, Salt Lake City, Utah 84112, USA*

Anode-supported solid oxide fuel cells (SOFCs) with Ni+yttria-stabilized zirconia (YSZ) anode, YSZ-samaria-doped ceria (SDC) bilayer electrolyte, and Sr-doped $LaCoO_3$ (LSC)+SDC cathode were fabricated. Fuel used consisted of $H_2$ diluted with He, $N_2$, $H_2O$, or $CO_2$, mixtures of $H_2$ and CO, and mixtures of CO and $CO_2$. Cell performance was measured at 800°C with the above-mentioned fuel gas mixtures and air as oxidant. For a given concentration of the diluent, cell performance was higher with He as the diluent than with $N_2$ as the diluent. Mass transport through porous Ni-YSZ anode for $H_2$-$H_2O$, CO-$CO_2$ binary systems, and $H_2$-$H_2O$-diluent gas ternary systems was analyzed using multicomponent gas diffusion theory. At high concentrations of diluent, the maximum achievable current density was limited by the anodic concentration polarization. From this measured limiting current density, the corresponding effective gas diffusivity was estimated. Highest effective diffusivity was estimated for fuel gas mixtures containing $H_2$-$H_2O$-He mixtures (~0.55 $cm^2/s$), and the lowest for CO-$CO_2$ mixtures (~0.07 $cm^2/s$). The lowest performance was observed with CO-$CO_2$ mixture as a fuel, which in part was attributed to the lowest effective diffusivity of the fuels tested and higher activation polarization.
 [DOI: 10.1149/1.1579480] 

Manuscript submitted April 21, 2002; revised manuscript received January 20, 2003. Available electronically May 30, 2003.

Recent work has demonstrated that anode-supported solid oxide fuel cells (SOFCs) exhibit high performance at intermediate temperatures. Maximum power densities as high as 1.8-1.9 $W/cm^2$ have been reported at 800°C for anode-supported single cells.[1-4] In a typical anode-supported SOFC, the anode support is a Ni-yttria-stabilized zirconia (YSZ) cermet between ~0.5 and 2 mm thick. The electrolyte is a thin (~10 μm), dense YSZ film supported on a porous anode substrate. The cathode is usually a porous mixture of strontium-doped manganite, $La_{1-x}Sr_xMnO_{3-\delta}$ (LSM), and YSZ,[1-3] or a porous mixture of strontium-doped cobaltite, $La_{1-x}Sr_xCoO_{3-\delta}$ (LSC), and Sm-doped $CeO_2$ (SDC).[4] In addition, single-phase, mixed ionic-electronic conductors (MIEC) materials have also been used in high-performance fuel cells. The use of thin electrolyte film results in a relatively low ohmic contribution to the total cell resistance, which makes it possible to operate anode-supported SOFCs at 800°C or lower and thereby realize the benefits of a lower temperature operation, such as the use of inexpensive metallic interconnect. One of the potential benefits of SOFCs over low-temperature fuel cells, such as proton exchange membranes (PEMs) is fuel flexibility, because SOFCs can potentially operate on various fuels including hydrogen, carbon monoxide, methane, and other hydrocarbon fuels without the problem of CO poisoning. Recent work has also shown that it may be possible to operate SOFCs directly on a number of hydrocarbon fuels, without the necessity of reforming.[5-8] However, in anode-supported SOFCs, significant losses may occur due to the resistance to the transport of fuel gas through a relatively thick anode, and especially at high fuel utilizations. The losses at the anode are expected to become even more severe when the fuel used contains gaseous species of molecular weights much greater than that of hydrogen ($H_2$), such as CO, $CH_4$, or other hydrocarbons. It is thus imperative that a thorough investigation of the transport characteristics of various gaseous species through porous anodes be conducted to fully assess anodic concentration polarization losses in anode-supported SOFCs. Gas transport through porous bodies, and the effects of parameters such as volume fraction porosity, morphology of pores, and pore size, have been studied in great detail.[9,10] However, there is limited information available in the literature pertaining to SOFCs.

Insofar as SOFCs are concerned, there are only a couple of papers in the literature examining gas-transport phenomena in porous anodes with emphasis on hydrocarbon fuels. Lehnert *et al.*[11] conducted a simulation study of gas transport coupled with steam-reforming and gas shift reactions in a Ni-YSZ porous anode using a single-channel model. The study showed that the anode structural parameter, defined as the ratio of porosity, $V_v$, to tortuosity, $\tau$, had a significant effect on methane conversion rate. A reduction of the structural parameter by 26% lowered the methane conversion by 12%. No electrochemical overpotential or performance measurements, however, were correlated with gas transport in this study. Yakabe *et al.*[12] studied gas transport in $H_2$-$H_2O$ and CO-$CO_2$ binary systems through porous anodes. Under a constant current density, the concentration distributions of reactants $H_2$ and CO along the direction normal and parallel to the electrode/electrolyte interface were evaluated. The results showed that the calculated concentration polarization was much higher for CO-$CO_2$ than for $H_2$-$H_2O$ due to the much lower diffusivity of CO-$CO_2$. These computational results were also compared with experimental measurements. The results on steam-reformed methane as fuel indicated that the gas shift reaction in porous anodes effectively reduces concentration polarization.

In the present paper, we address mass transport in porous anode support of an SOFC. Studies were conducted on a variety of fuel mixtures, such as as-received $H_2$; mixtures of $H_2$ with inert gases such as He, and $N_2$; $H_2$-$H_2O$, $H_2$-CO, and $H_2$-$CO_2$ mixtures; and CO-$CO_2$ mixtures. All tests were conducted on one cell to ensure that possible differences due to cell-to-cell variations are eliminated. Mass transport in these binary and ternary systems was analyzed. This included the estimation of effective diffusivities of gaseous species through porous anodes, the effect of diluents on transport, and the associated concentration polarization. In the case of mixtures of CO and $H_2$, the effect of *in situ* gas shift reaction was examined.

## Experimental

*Cell fabrication.*—While only measurements on one cell are reported, a number of cells were fabricated. Single cells consisted of a Ni+YSZ anode substrate, a Ni+YSZ anode interlayer, a YSZ-SDC bilayer thin-film electrolyte, a LSC+SDC cathode interlayer, and a LSC cathode current collector layer. The procedure for preparing an anode substrate and an anode interlayer was described elsewhere in detail[13] and is briefly described here. NiO and YSZ powders from commercial sources were mixed in requisite proportions and ball-milled in alcohol, dried, and screened through a 150 mesh sieve. A circular disk ~1.2 mm thick and ~3 cm diam was uniaxially die-pressed and presintered at 1000°C for 1 h. The disk was then coated with a slurry of NiO+YSZ anode interlayer and fired again at the same temperature for 1 h to form a NiO+YSZ interlayer ~20 μm thick. YSZ and SDC layers were applied on the anode interlayer

* Electrochemical Society Active Member.
z E-mail: anil.virkar@m.cc.utah.edu

surface sequentially using YSZ and SDC suspensions made from YSZ and 20 mol% samarium-doped $CeO_2$ powders, dispersed ultrasonically in appropriate amounts of suitable liquids. Then the bilayer electrolyte-anode substrate assembly was sintered in air at a temperature between 1400 and 1500°C to form a dense, well-bonded YSZ-SDC bilayer electrolyte-anode structure. The thickness of the SDC layer was around 3 μm and the total thickness of the YSZ-SDC bilayer electrolyte thin film was ~10 μm. The thin SDC layer, as part of the electrolyte, served as a barrier, which prevented a direct contact between YSZ and LSC. In this manner, the possible chemical reaction between YSZ and LSC, which can form insulating $La_2Zr_2O_7$ during a high-temperature firing step, could be prevented.

The porous cathode interlayer was a composite of 50 wt % strontium-doped lanthanum cobaltite [$La_{1-x}Sr_xCoO_{3-\delta}$ (LSC), $x$ = 0.3-0.7] and 50 wt % SDC. The cathode interlayer was applied by screen-printing, followed by firing at a temperature between 1050 and 1300°C for 2 h to form a good bond between the SDC layer and the cathode interlayer. The thickness of the interlayer after firing was ~20 μm. On top of the interlayer, a porous layer of LSC was applied, followed by firing at a temperature between 1050 and 1300°C for 1 h in air. The final anode thickness and the disk diameter were 1.1 and 27.7 mm, respectively. The cathode area was 1.1 $cm^2$.

*The measurement of cell performance*.—The cell was mounted in a test fixture, which consisted of an alumina tube and an alumina ring. The cell was secured between the alumina tube and the alumina ring and spring-loaded to ensure good sealing between the cell and the alumina tube using a flexible gasket. A silver mesh and a Ni mesh, used as current collectors at the cathode and the anode, respectively, were spring-loaded against, respectively, the cathode and the anode. Measurements were carried out at 800°C, at 1 atm total pressure (both fuel and air), and at predetermined, constant total flow rates of fuel or fuel mixture and of air. The cell was reduced *in situ* at 800°C in a 10% $H_2$ + 90% $N_2$ mixture for several hours prior to measurements. The fuel flow rate was maintained at 140 mL/min and the air flow rate was maintained at 550 mL/min in all experiments. Open-circuit potentials (OCPs) were measured under constant fuel flow over the anode and the airflow over the cathode.

Cell performance was measured using various fuel gas mixtures, which included as-received $H_2$ (straight from the as-received cylinders, 99.99% pure $H_2$), as-received CO (straight from the as-received cylinders, 99.99% pure CO), $H_2$ + CO mixtures, $H_2$ diluted with He, $N_2$, $CO_2$, $H_2O$, and CO diluted with $CO_2$. Current-voltage (I-V) curves were measured at various diluent concentrations, *i.e.*, at various partial pressures of the diluent, while the total flow rate of fuel mixture was kept constant. Current densities were calculated based on the cathode area. The fact that cathode area is different from the anode surface exposed to fuel introduces a small error (typically <10%) in the power density. This issue has been addressed in detail elsewhere.[13] Cell tests with as-received hydrogen were conducted without bubbling through a water bubbler.

*Cell characterization*.—Porosity of the Ni-YSZ anode was measured using the Archimedes method. The tested cell was broken into several small pieces. Dry weight, $W_{dry}$, wet weight, $W_{wet}$, and weight in water, $W_{water}$, were measured using a high-accuracy balance. Wet weight was measured (in air) soon after the surface of the sample was wiped dry, after boiling in water for 2 h. Porosity was calculated according to the equation

$$\text{Porosity} = \frac{W_{wet} - W_{dry}}{W_{wet} - W_{water}} \quad [1]$$

One of the fractured pieces was evacuated (to remove air from the pores) and impregnated with an epoxy. After hardening the epoxy, the sample was polished down to 1 μm finish. The microstructure of the cell was examined using scanning electron microscopy (SEM) and the mean pore radius was determined by quantitative stereology.[14]

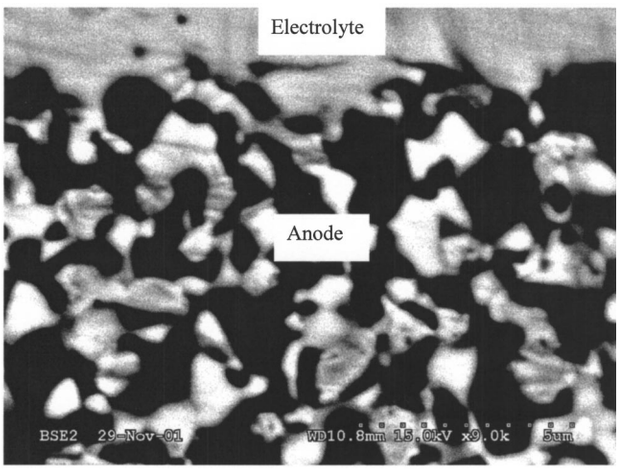


**Figure 1.** An SEM micrograph of a polished section of the Ni+YSZ anode (after impregnating with an epoxy).

## Results

An SEM micrograph of a polished section of the Ni-YSZ anode is shown in Fig. 1. Figures 2-4 show cell voltage *vs.* current density, and power density *vs.* current density traces with as-received $H_2$, and $H_2$ diluted with various concentrations of He, $N_2$, and $CO_2$. For as-received $H_2$ as the fuel, the OCP was around 1.05 V, the maximum power density was about 1.7 W/$cm^2$, and there was no obvious limiting current density, even at the highest current density of 4.5 A/$cm^2$ at which measurements were made. When $H_2$ was diluted with various diluents, the general trend was similar for each diluent, namely: (*i*) with increasing dilution the open-circuit voltage (OCV) decreased, and (*ii*) the maximum power density as well as the maximum current density decreased. At high diluent concentrations, substantial concentration polarization was present as evidenced by the observation of a limiting current density. Since the cathode conditions were kept the same, the observed changes in performance with different diluents and their concentrations could be solely attributed to changes made in anodic conditions.

A comparison of Fig. 2 ($H_2$-He), 3 ($H_2$-$N_2$), 4 ($H_2$-$CO_2$), and 5 ($H_2$-$H_2O$) shows that the maximum power density achieved at the highest concentration of the diluent (~78-81%) was the highest for $H_2$-He mixtures (~0.75 W/$cm^2$) and the lowest for $H_2$-$CO_2$ mixtures (~0.3 W/$cm^2$). Also, the corresponding short-circuit current

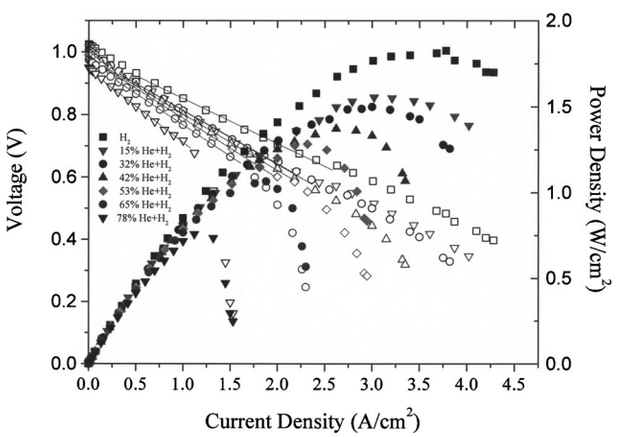


**Figure 2.** Voltage and power density *vs.* current density at 800°C with as-received $H_2$ and $H_2$ diluted with He as fuel.

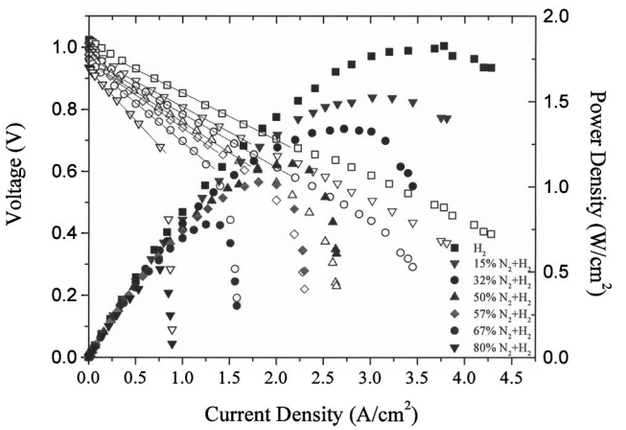


**Figure 3.** Voltage and power density *vs.* current density at 800°C with as-received $H_2$ and $H_2$ diluted with $N_2$ as fuel.

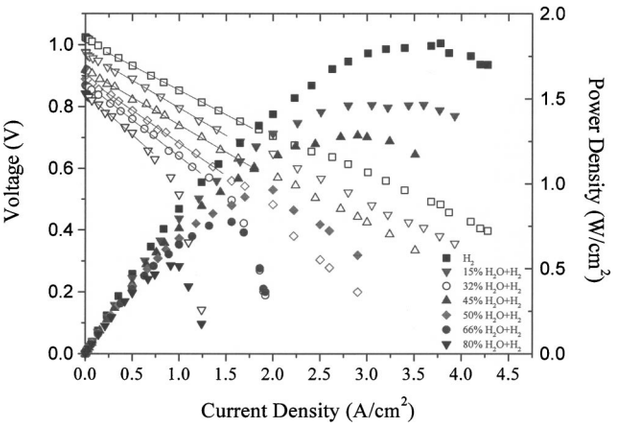


**Figure 5.** Voltage and power density *vs.* current density at 800°C for $H_2$-$H_2O$ binary system with various concentrations of $H_2O$.

density was the highest for $H_2$-He mixture (~1.55 A/cm$^2$) and the lowest for $H_2$-$CO_2$ mixture (~0.7 A/cm$^2$). The highest power density measured was ~1.7 W/cm$^2$ for this cell with as-received $H_2$ as the fuel. A comparison of $H_2$-He and $H_2$-$N_2$ mixtures, wherein the diluent is inert, shows that the maximum power density at the highest diluent concentration is ~0.75 W/cm$^2$ for $H_2$-He and ~0.5 W/cm$^2$ for $H_2$-$N_2$ mixtures. Also, the corresponding anode-limiting current densities were ~1.55 A/cm$^2$ for $H_2$-He mixture and ~0.85 A/cm$^2$ for $H_2$-$N_2$ mixture of similar diluent concentrations.

As seen in Fig. 4 and 5, the OCV exhibited a stronger dependence on the diluent concentration when the diluent was either $CO_2$ or $H_2O$, consistent with expectations as the diluents in these cases are not inert, and enter into chemical reactions of the following type

In $H_2$-$H_2O$ mixtures

$$H_2 + \tfrac{1}{2}O_2 \Leftrightarrow H_2O$$

and in $H_2$-$CO_2$ mixtures

$$H_2 + CO_2 \Leftrightarrow H_2O + CO$$

until the respective reaction equilibria are established.

Figure 6 shows cell performance curves for gas mixtures containing CO and $CO_2$ as the fuel. The maximum power density measured with as-received CO as the fuel was ~0.7 W/cm$^2$, which is considerably lower than that with as-received $H_2$ as the fuel (Fig. 2-5). For the gas mixture containing 18% CO+82% $CO_2$, the maximum power density was only ~0.1 W/cm$^2$, and the corresponding limiting current density was only ~0.2 A/cm$^2$. An examination of Fig. 2-6 shows that a limiting current behavior is observed in all cases at higher diluent concentrations. The limiting current density, $i_{as}$, for each case is plotted *vs.* the partial pressure of the fuel gas (either $H_2$ or CO) in Fig. 7. It is seen that the dependence of $i_{as}$ on the respective partial pressure ($p_{H_2}$ or $p_{CO}$) is close to linear, with $H_2$-He fuel (or $H_2$-$H_2O$-He mixtures) exhibiting the highest $i_{as}$ and the highest slope, and the CO-$CO_2$ mixtures exhibiting the lowest $i_{as}$ and the lowest slope.

Figure 8 shows the performance curves with $H_2$ + CO gas mixtures as the fuel, where the composition was varied between ~100% (as-received) $H_2$ and ~100% (as-received) CO. The OCV is essentially independent of the relative proportions of $H_2$ and CO. The maximum power density varied between ~1.7 W/cm$^2$ for 100% $H_2$ to ~0.7 W/cm$^2$ for 100% CO. Note that the maximum power density for CO concentrations less than ~55% ranges between ~1.5 and ~1.7 W/cm$^2$; and for CO concentrations between 68 and 100%, the maximum power density ranges between ~1.2 and ~0.7 W/cm$^2$.

## Discussion

*Thermodynamic calculation of OCVs.*—The thermodynamic OCV of a fuel cell, which is the Nernst potential, is given by

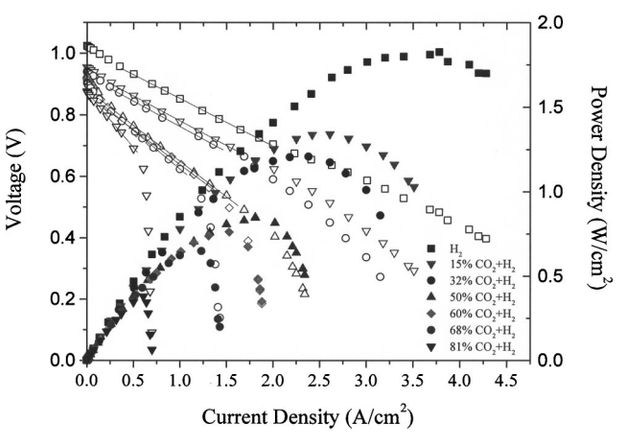


**Figure 4.** Voltage and power density *vs.* current density at 800°C with as-received $H_2$ and $H_2$ diluted with $CO_2$ as fuel.

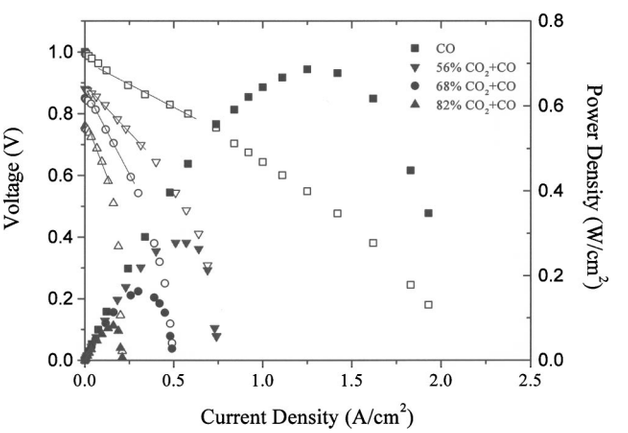


**Figure 6.** Voltage and power density *vs.* current density at 800°C for CO-$CO_2$ binary system with various concentrations of $CO_2$.

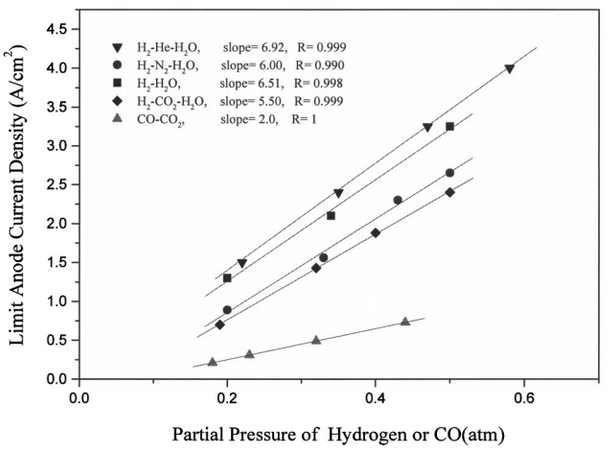


**Figure 7.** Anode limiting current density *vs.* partial pressure of $H_2$ or CO at 800°C.

$$E = \frac{RT}{4F}\ln\left(\frac{p_{O_{2(cathode)}}}{p_{O_{2(anode)}}}\right) \quad [2]$$

where $p_{O_{2(cathode)}}$ is the partial pressure of oxygen at the cathode (under open-circuit conditions), which is 0.21 atm when air is used as the oxidant; $p_{O_{2(anode)}}$ is the partial pressure of oxygen in fuel at the anode (under open-circuit conditions). For example, when $H_2$ is the fuel

$$H_2 + \frac{1}{2}O_2 \Leftrightarrow H_2O \quad [3]$$

at equilibrium, the partial pressure of oxygen at the anode, $p_{O_{2(anode)}}$ is given as

$$\ln p_{O_{2(anode)}} = \frac{2\Delta G_3^o}{RT} + 2\ln\left(\frac{p_{H_2O}}{p_{H_2}}\right) \quad [4]$$

where $\Delta G_3^o$ is the standard free energy of Reaction 3. The $\Delta G_3^o$ is $-188.165$ kJ/mol at 800°C.[15] At various partial pressures of $H_2$ and $H_2O$, $p_{O_{2(anode)}}$ can be calculated from Eq. 4 and the OCV can be determined using Eq. 2.

Figure 9 shows the calculated $p_{O_{2(anode)}}$ (except for as-received

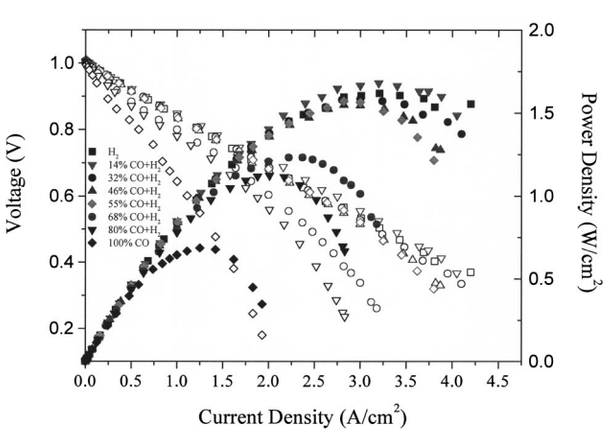


**Figure 8.** Voltage and power density *vs.* current density at 800°C for $H_2$-CO mixtures as fuel with various concentrations of CO.

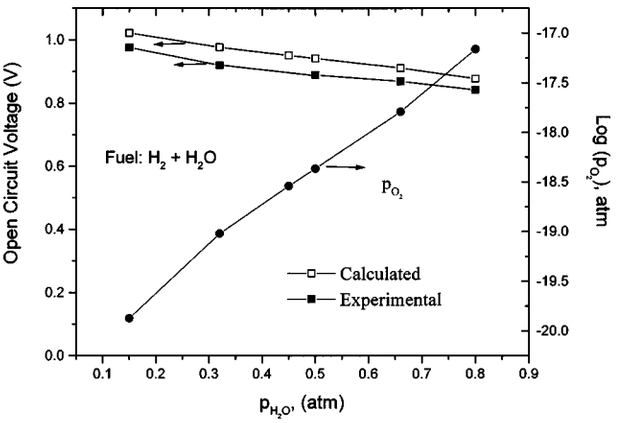


**Figure 9.** Partial pressure of oxygen at the anode and OCV as a function of $p_{H_2O}$ for $H_2$-$H_2O$ at 800°C.

$H_2$, whose water content was not known), the calculated OCV, and the experimentally measured OCV as a function of $p_{H_2O}$. The partial pressure of oxygen at the anode increases from $10^{-20}$ atm to $10^{-17}$ atm, and the calculated OCV decreases from 1.021 to 0.877 V, when the $p_{H_2O}$ increases from 0.15 to 0.8 atm. The measured OCV, in general, exhibits the same trend as the calculated one, although it is about 50 mV lower than the calculated OCV. For the reaction

$$CO + \tfrac{1}{2}O_2 \Leftrightarrow CO_2 \quad [5]$$

the standard free energy, $\Delta G_5^o$, is $-189.65$ kJ/mol.[15] At $p_{CO}$ lower than 0.8 atm, the disproportionation reaction

$$2CO \Leftrightarrow CO_2 + C \quad [6]$$

for which the standard free energy change is $\Delta G_6^\circ = 17.63$ kJ/mol,[15] should not occur at 800°C and 1 atm pressure, based on a thermodynamic calculation. For values of $p_{CO}$ less than 0.8 atm, the partial pressures of CO and $CO_2$ in the initial gas mixture were used to estimate the equilibrium partial pressure of oxygen at the anode, namely, $p_{O_{2(anode)}}$, using the following equation

$$\ln p_{O_{2(anode)}} = \frac{2\Delta G_5^o}{RT} + 2\ln\left(\frac{p_{CO_2}}{p_{CO}}\right) \quad [7]$$

For values of $p_{CO}$ greater than 0.8 atm, first the partial pressures of CO and $CO_2$ according to the disproportionation reaction, Reaction 6, were estimated. Then $p_{O_{2(anode)}}$ was estimated using the corresponding values of the partial pressures of CO and $CO_2$ and Eq. 7. Finally, the OCV was calculated as a function of the partial pressure of $CO_2$ in the initial mixture, $p^o_{CO_2}$. The calculated $p_{O_{2(anode)}}$, the calculated OCV, and the measured OCV are plotted as a function of $p^o_{CO_2}$ in Fig. 10. The trends in the measured OCV and the calculated OCV are similar, although the measured OCV is between 50 and 75 mV lower than the theoretical values.

For calculating $p_{O_{2(anode)}}$ and OCV for $H_2 + CO_2$ gas mixtures as the fuel, the reverse gas shift reaction, namely

$$H_2 + CO_2 \Leftrightarrow H_2O + CO \quad [8]$$

for which the standard free energy is $\Delta G_8^o = 0.385$ kJ/mol at 800°C was considered. The corresponding equilibrium $p_{CO}$, $p_{CO_2}$, $p_{H_2}$, and $p_{H_2O}$ were calculated. Then the corresponding $p_{O_{2(anode)}}$ was calculated using either the $H_2$-$H_2O$ equilibrium or the CO-$CO_2$ equilibrium. Using the calculated $p_{O_{2(anode)}}$, the OCV was estimated by

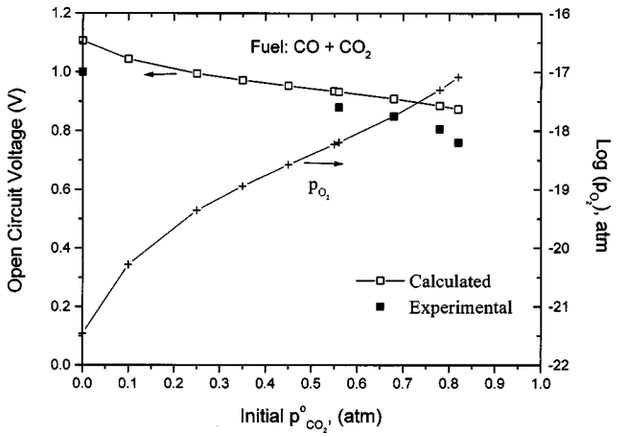


**Figure 10.** Partial pressure of oxygen at the anode and OCV as a function of $p_{CO_2}$ for CO-$CO_2$ at 800°C.

Eq. 2. The calculated $p_{O_{2(anode)}}$, the calculated OCV, and the measured OCV are plotted as a function of the partial pressure of $CO_2$ in the initial gas mixture, $p^{o}_{CO_2}$, in Fig. 11. As seen in the figure, the calculated and the measured OCV are in good agreement, especially for higher values of $p^{o}_{CO_2}$.

The thermodynamic calculations and comparison with experimental results show generally reasonable agreement between the calculated and experimental OCV values, insofar as the trends are concerned. However, the experimental values of the OCV are typically about 50 mV lower, and in some cases as much as 100 mV lower. There are a couple of possibilities for this discrepancy. (*i*) There may have been a few pinholes in the YSZ film. (*ii*) The sealing may not have been perfect. A lower OCV thus would imply a higher $H_2O$ or $CO_2$ pressure and a correspondingly higher partial pressure of oxygen at the anode, $p_{O_{2(anode)}}$. Leakage is also the possible reason that OCV in $H_2$-He and $H_2$-$N_2$ mixtures is dependent upon the relative proportions of $H_2$ and inert gas. If there had been no leakage, ideally, it would be expected that the OCV would be essentially independent of the concentration of inert diluent, He or $N_2$. In principle, using the measured OCV, this $p_{O_{2(anode)}}$ can be calculated and thus the relative amount of water (or $CO_2$) present in the fuel can be estimated. However, as the general trend in measured OCV is consistent with calculations (and expectations) and significant uncertainties may exist in such calculations, no corrections for leakage were made, and the data reported are as measured.

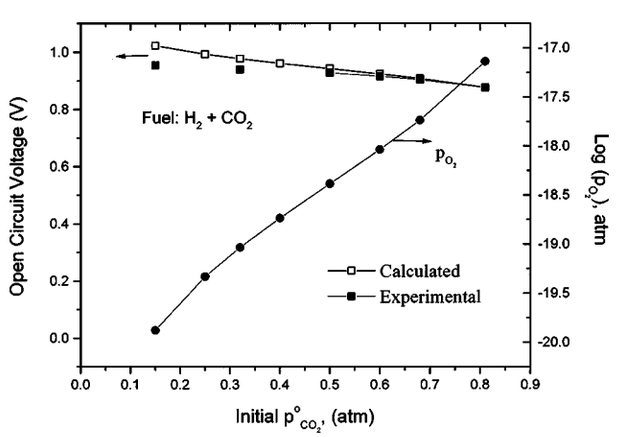


**Figure 11.** Partial pressure of oxygen at the anode and OCV as a function of $p_{H_2}$ for $H_2$-$CO_2$ at 800°C.

*Gas transport in porous anodes*.—Gas transport through porous electrodes and correlation with electrochemical performance for binary gases, $H_2$-$H_2O$ in the anode and $O_2$-$N_2$ in the cathode, have been addressed in detail.[2] There are two main fluxes contributing to mass transport in a porous electrode: a diffusive and a viscous flux. In general, the viscous flow, which is driven by a pressure gradient, is negligible compared to the diffusive flow in porous electrodes. Therefore, gas transport in porous electrodes is mainly due to diffusion, which includes free molecular or Knudsen flow, and a continuum flow.

The general diffusion process for a multicomponent gas system is described by the Stefan-Maxwell equation

$$\frac{N_i}{D_{K,i}} + \sum_{\substack{j=1 \\ j\neq i}} \frac{X_j N_i - X_i N_j}{D_{ij}} = -\frac{P}{RT}\frac{dX_i}{dx} \qquad [9]$$

where $N_i$ and $N_j$ are molar fluxes of components i and j (no. mol/cm$^2$ s), respectively, $D_{K,i}$ and $D_{ij}$ are the Knudsen diffusion coefficient for component i and the binary diffusion coefficient for components i and j, respectively, $X_i$ and $X_j$ are the mole fractions of components i and j, respectively, $P$ is the total pressure, $R$ is the gas constant, $T$ is the absolute temperature, and $x$ is the coordinate along the diffusion direction. Knudsen diffusion is due to molecule-to-wall collision, which predominates over molecule-to-molecule collision when the pore size is smaller than the mean free path.[10] The Knudsen diffusion coefficient can be computed according to the kinetic theory of gases, using the following formula

$$D_{K,i} = \frac{2}{3}\left(\frac{8RT}{\pi M_i}\right)^{1/2}\bar{r} \qquad [10]$$

where $\bar{r}$ is the mean pore radius and $M_i$ is the molecular weight of the diffusing gas. The binary diffusion coefficient, $D_{ij}$, is generally experimentally measured or calculated using the Chapman-Enskog equation,[16] if it is not available experimentally. According to the Chapman-Enskog model, the binary diffusion coefficient in cm$^2$/s is given by[16]

$$D_{ij} = \frac{1.86 \times 10^{-3} T^{3/2}\left(\frac{1}{M_i} + \frac{1}{M_j}\right)^{1/2}}{p\Omega\sigma_{ij}^2} \qquad [11]$$

where $\Omega$ is the collision integral (dimensionless), $\sigma_{ij}$ is the average collision diameter (in angstroms), $M_i$ and $M_j$ are molecular weights of component i and j, respectively, and $P$ is the total pressure (in atm). Using $\Omega$ and $\sigma_{ij}$ data from Cussler,[16] the calculated $D_{ij}$ for various gaseous species and at several temperatures are listed in Table I, along with some experimental values from the literature for comparison.[15,17,18] Slight difference, usually less than 10%, is often observed between the calculated values and the experimental values over a range of temperatures between room temperature and 473 K. Little data are available at higher temperatures. Hence, $D_{ij}$ at 800°C were estimated using the Chapman-Enskog model.

In the present experiments, the mean pore radius of the Ni-YSZ electrode was estimated from SEM micrographs (Fig. 1) to be ~0.5 μm. The calculated Knudsen diffusion coefficients at 800°C for $H_2$ and CO through the Ni-YSZ porous electrode are 11.3 and 3 cm$^2$/s, respectively. These values are comparable to the respective binary diffusion coefficient of $H_2$-He, which is 13.3 cm$^2$/s, and CO-$CO_2$, which is 1.41 cm$^2$/s at the same temperature (Table I). This indicates that Knudsen diffusion is an important process in the present porous anodes with 0.5 μm mean pore radius and should be taken into account.

For a ternary system such as $H_2$-He-$H_2O$, the $H_2$ molar flux from Eq. 9 is given by

**Table I. Calculated binary diffusion coefficients from the Chapman-Enskog equation and comparison with some experimental data from the literature.**

| $D_{ij}$ ($cm^2/s$) | $H_2$-He | $H_2$-$N_2$ | $H_2$-$CO_2$ | $H_2$-$H_2O$ | $H_2$-CO | CO-$CO_2$ |
|---|---|---|---|---|---|---|
| 293K | 1.535 | 0.722 | 0.604 | 0.738 | 0.726 | 0.149 |
| | 1.53[a] | 0.728[a] | 0.651[b] | 0.834[b] | 0.735[a] | 0.162[c] |
| | 1.49[c] | 0.772[c] | | | 0.772[c] | |
| 473K | 3.417 | 1.626 | 1.395 | 1.819 | 1.642 | 0.349 |
| | 3.45[a] | 1.631[a] | 1.513[b] | 1.996[b] | 1.651[a] | 0.384[c] |
| | 3.39[c] | 1.743[c] | 1.473[c] | | 1.743[c] | |
| 1073K | 13.29 | 6.303 | 5.56 | 7.704 | 6.373 | 1.408 |

[a] From Ref. 17.
[b] From Ref. 18.
[c] From Ref. 15.

$$\frac{N_{H_2}}{D_{K,H_2}} + \frac{X_{He}N_{H_2} - X_{H_2}N_{He}}{D_{H_2,He}} + \frac{X_{H_2O}N_{H_2} - X_{H_2}N_{H_2O}}{D_{H_2,H_2O}} = -\frac{P}{RT}\frac{dX_{H_2}}{dx} \quad [12]$$

Under steady-state conditions, $N_{H_2O} = -N_{H_2}$ and $N_{He} = 0$. Thus

$$N_{H_2}\left(\frac{1}{D_{K,H_2}} + \frac{X_{He}}{D_{H_2,He}} + \frac{1 - X_{He}}{D_{H_2,H_2O}}\right) = -\frac{P}{RT}\frac{dX_{H_2}}{dx} \quad [13]$$

From Eq. 13, $H_2$ flux can be written in a similar form as Fick's equation by

$$N_{H_2} = -\frac{PD_{H_2}}{RT}\frac{dX_{H_2}}{dx} \quad [14]$$

where $D_{H_2}$ is defined as the $H_2$ diffusion coefficient in the $H_2$-$H_2O$-He ternary system, and is given by

$$D_{H_2} = \left(\frac{1}{D_{K,H_2}} + \frac{X_{He}}{D_{H_2,He}} + \frac{1 - X_{He}}{D_{H_2,H_2O}}\right)^{-1} \quad [15]$$

When $X_{He} = 0$, *i.e.*, for $H_2$-$H_2O$ binary system, the $H_2$ diffusion coefficient becomes

$$D_{H_2} = \left(\frac{1}{D_{K,H_2}} + \frac{1}{D_{H_2,H_2O}}\right)^{-1} \quad [16]$$

Similarly, for the CO-$CO_2$ binary system, the CO diffusion coefficient is given by

$$D_{CO} = \left(\frac{1}{D_{K,CO}} + \frac{1}{D_{CO,CO_2}}\right)^{-1} \quad [17]$$

where $D_{K,CO}$ and $D_{CO,CO_2}$ are the Knudsen diffusion coefficient of CO and the binary diffusion coefficient of CO-$CO_2$, respectively.

The preceding equations for diffusion coefficients are for transport in a multicomponent gas system and do not account for the volume fraction of porosity and the tortuous nature of path through porous bodies. When the transport occurs through a porous body, the interaction of gaseous species with the porous matrix must be included. The simplest approach for taking this into account is to modify the diffusion coefficients by the volume fraction porosity, $V_v$, and the tortuous nature of the actual transport, characterized by the so-called tortuosity factor, $\tau$.[16] The resulting diffusion coefficients or diffusivities are termed effective diffusion coefficients or effective diffusivities. For $H_2$ and CO, the corresponding effective diffusivities are given by[16]

$$D_{H_2,eff} = \frac{V_v}{\tau}D_{H_2} \quad [18]$$

and

$$D_{CO,eff} = \frac{V_v}{\tau}D_{CO} \quad [19]$$

where $D_{H_2}$ and $D_{CO}$ are given, respectively, by Eq. 15 or 16 and 17.

As shown on the right side of Eq. 15, for a ternary system $D_{H_2}$ is not only a function of diffusion coefficients, $D_{K,H_2}$, $D_{H_2,He}$, and $D_{H_2,H_2O}$, but is also a function of the mole fraction of the diluent gas, $X_{He}$. If $X_{He}$ varies from position to position along the diffusion direction, $D_{H_2}$ will be a function of position. The variation of $X_{He}$ as a function of the position, $x$, can be determined by solving Eq. 9 for the He flux, $N_{He}$, given by

$$\frac{N_{He}}{D_{K,He}} + \frac{X_{H_2}N_{He} - X_{He}N_{H_2}}{D_{He,H_2}} + \frac{X_{H_2O}N_{He} - X_{He}N_{H_2O}}{D_{He,H_2O}} = -\frac{P}{RT}\frac{dX_{He}}{dx} \quad [20]$$

Because the net flow of He, $N_{He}$, is zero and $N_{H_2} = -N_{H_2O}$ in steady state, Eq. 20 becomes

$$N_{H_2}\left(\frac{1}{D_{He,H_2O}} - \frac{1}{D_{He,H_2}}\right)X_{He} = -\frac{P}{RT}\frac{dX_{He}}{dx} \quad [21]$$

Integration of Eq. 21 gives

$$X_{He}^{l_a} = X_{He}^{o}\exp\left[\frac{RTN_{H_2}l_a}{P}\left(\frac{1}{D_{He,H_2}} - \frac{1}{D_{He,H_2O}}\right)\right] \quad [22]$$

where $l_a$ is the anode thickness, $X_{He}^{\circ}$ is the mole fraction of He at $x = 0$, and $X_{He}^{l_a}$ is the mole fraction of He at $x = l_a$. The case of interest is that of a porous anode. Thus, the diffusivities must be those corrected for porosity and tortuosity factor. Thus, the applicable equation is actually

$$X_{He}^{l_a} = X_{He}^{o}\exp\left[\frac{RTN_{H_2}l_a}{P}\left(\frac{1}{D_{He,H_2,eff}} - \frac{1}{D_{He,H_2O,eff}}\right)\right] \quad [23]$$

Equation 22 and 23 show that $X_{He}$ varies exponentially as a function of position. For the case of transport through space, in the absence of a porous body, the calculated variation of $X_{He}$ along the electrode is very small. Using the estimated diffusion coefficients from the Chapman-Enskog model, $D_{He,H_2} = 13.29$ $cm^2/s$ and $D_{He,H_2O} = 4.07$ $cm^2/s$, the $X_{He}$ at the electrode/electrolyte interface ($l_a = 0.1$ cm) is about 0.8% lower than the bulk molar value of He, $X_{He}^{\circ}$, at a current density of 1 $A/cm^2$, *i.e.*, for a molar flux of $5.18 \times 10^{-6}$ $mol/cm^2s$. Even at a current density close to the anode limiting current density, 3 $A/cm^2$, $X_{He}$ is only 3% lower than $X_{He}^{\circ}$. Such, however, is not the case for a porous body. For transport through porous anodes, Eq. 23 must be used. The corresponding variation in $X_{He}$ is ~10% at a current density of 1 $A/cm^2$ and ~20% at a current density of 3 $A/cm^2$. Though this variation is not insignificant, for simplicity we neglect this aspect and assume that the diffusion coefficient of $H_2$ is independent of position.

If the electrode microstructure is not a function of position, *i.e.*, $V_v$ and $\tau$ are constant, integration of Eq. 14, using effective diffusivities, gives a simple equation for $H_2$ flux in a ternary system, similar to that for a binary system, namely

$$N_{H_2} = -\frac{PD_{H_2,\text{eff}}}{RTl_a}(X_{H_2} - X'_{H_2}) \quad [24]$$

where $X'_{H_2}$ and $X_{H_2}$ are the mole fractions of $H_2$ over the anode surface ($x = 0$) and at the anode/electrolyte interface ($x = l_a$), and $D_{H_2,\text{eff}}$ is the effective ternary diffusion coefficient as defined by Eq. 15 and 18. Replacing mole fractions with partial pressures, Eq. 24 becomes

$$N_{H_2} = -\frac{D_{H_2,\text{eff}}}{RTl_a}(p_{H_2} - p'_{H_2}) \quad [25]$$

where $p'_{H_2}$ and $p_{H_2}$ are the partial pressure of $H_2$ over the anode surface ($x = 0$) and the partial pressure of $H_2$ at the anode/electrolyte interface ($x = l_a$), respectively. Assuming gases are well mixed above the anode, similar to the situation in a continuously stirred tank reactor (CSTR), $p'_{H_2}$ is given by

$$p'_{H_2} = p^o_{H_2} - \frac{N_{H_2}A}{m_T}P \quad [26]$$

where $p^o_{H_2}$ is the initial (incoming fuel) partial pressure of $H_2$, $A$ is the electrode area (1.1 $cm^2$), $m_T$ the total molar flow rate of fuel and diluent, and $P$ is total pressure. Substituting for $p'_{H_2}$ from Eq. 26 into Eq. 25 gives

$$N_{H_2} = -\frac{D_{H_2,\text{eff}}}{RTl_a}\left(p_{H_2} - p^o_{H_2} + \frac{N_{H_2}A}{m_T}P\right) \quad [27]$$

Rearranging Eq. 27, $H_2$ molar flux is given by

$$N_{H_2} = -\frac{\dfrac{D_{H_2,\text{eff}}(p_{H_2} - p^o_{H_2})}{RTl_a}}{1 + \dfrac{D_{H_2,\text{eff}}}{RTl_a}\dfrac{AP}{m_T}} \quad [28]$$

A maximum in $H_2$ flux occurs when $p_{H_2}$ at the interface approaches zero. This maximum flux is given by

$$N_{H_2,\max} = \frac{\dfrac{D_{H_2,\text{eff}}p^o_{H_2}}{RTl_a}}{1 + \dfrac{D_{H_2,\text{eff}}}{RTl_a}\dfrac{AP}{m_T}} \quad [29]$$

The net current density passing through the cell is related to the net hydrogen flux arriving at the anode/electrolyte interface, and is given by

$$i = 2FN_{H_2} = -\frac{\dfrac{2FD_{H_2,\text{eff}}(p_{H_2} - p^o_{H_2})}{RTl_a}}{1 + \dfrac{D_{H_2,\text{eff}}}{RTl_a}\dfrac{AP}{m_T}} \quad [30]$$

For the maximum possible hydrogen flux given by Eq. 29, there will be a corresponding maximum in current density, which is the anode limiting current density given by

$$i_{as} = \frac{\dfrac{2FD_{H_2,\text{eff}}p^o_{H_2}}{RTl_a}}{1 + \dfrac{D_{H_2,\text{eff}}}{RTl_a}\dfrac{AP}{m_T}} \quad [31]$$

In all experiments, when the mole percent of the diluent was more than 40%, a limiting current density was observed. From the experimentally measured anode limiting current density, one can estimate the effective diffusion coefficients for $H_2$ for several diluents and at various concentrations by rearranging Eq. 31 as follows

$$D_{H_2,\text{eff}} = \frac{i_{as}}{\dfrac{2Fp^o_{H_2}}{RTl_a} - \dfrac{i_{as}}{RTl_a}\dfrac{AP}{m_T}} \quad [32]$$

Also, for CO-$CO_2$ mixtures, Eq. 32 can be used with $p^o_{H_2}$ replaced by $p^o_{CO}$, and $D_{H_2,\text{eff}}$ replaced by $D_{CO,\text{eff}}$. Table II lists the calculated diffusion coefficients from Equation 15-17, the estimated effective $H_2$ (and CO) diffusion coefficients from Eq. 32, and the experimentally measured $i_{as}$ values from the voltage-current density polarization curves.

From Table II, it is seen that the $H_2$ diffusion coefficient, $D_{H_2}$, for $H_2$-$H_2O$ is about five times larger than that for CO-$CO_2$, $D_{CO}$. For $H_2$-$H_2O$, the effective diffusion coefficient estimated using Eq. 32, ranges from 0.470 to 0.506 $cm^2/s$, almost independent of gas composition, consistent with Eq. 16. For CO-$CO_2$ mixtures, it varies from 0.063 to 0.090 $cm^2/s$ over the range of $p_{CO}$ investigated. This suggests that mass transport of $H_2$ in $H_2$-$H_2O$ mixtures should be about five to six times faster than that of CO in CO-$CO_2$ mixtures. If CO is used as a fuel, the cell performance is expected to be lower than with $H_2$ as a fuel due to slow diffusion rate, regardless of other effects, such as the intrinsically low electrochemical activity of CO.

Prior work has shown that anodic concentration polarization for $H_2$-$H_2O$ gas mixtures is given by[2]

$$\eta_{conc} = -\frac{RT}{2F}\ln\left(1 - \frac{i}{i_{as}}\right) + \frac{RT}{2F}\ln\left(1 + \frac{p^o_{H_2}i}{p^o_{H_2O}i_{as}}\right) \quad [33]$$

It is readily seen that the corresponding equation for CO-$CO_2$ gas mixtures as a fuel is given by

$$\eta_{conc} = -\frac{RT}{2F}\ln\left(1 - \frac{i}{i_{as}}\right) + \frac{RT}{2F}\ln\left(1 + \frac{p^o_{CO}i}{p^o_{CO_2}i_{as}}\right) \quad [34]$$

Using Eq. 33 and 34,[a] $\eta_{conc}$ was calculated as a function of current density for a $H_2$-$H_2O$ mixture of composition 34% $H_2$ − 66% $H_2O$, and for a CO-$CO_2$ mixture of composition 32% CO−68% $CO_2$, for which the corresponding anode limiting current densities were ~2 and ~0.5 $A/cm^2$, respectively. The calculated concentration polarization is compared with the measured total polarization (by subtracting the ohmic contribution) in Fig. 12. It is readily seen that anodic concentration polarization is much greater in CO-$CO_2$ mixtures as compared to $H_2$-$H_2O$ mixtures. The difference between the measured total (excluding the ohmic) and the calculated anodic concentration polarization is attributed to anodic and cathodic acti-

[a] Since the partial pressure of $H_2$ or CO at the anode/fuel interface is a function of the current density (using Eq. 26), one must strictly use $p_{H_2}$ instead of $p^o_{H_2}$ (or $p_{CO}$ instead of $p^o_{CO}$) in estimating the concentration polarization and attribute the remainder of the terms to polarization associated with the depletion of fuel. Here, the two terms are combined into a single equation describing concentration polarization, namely, Eq. 33 for $H_2$ as a fuel (or Eq. 34 for CO as a fuel).

**Table II. Partial pressure of dilute gas, anode limiting current density, $H_2$ and CO diffusion coefficient, porosity, and tortuosity.**

**$H_2$-$H_2O$ Binary System**

| $p_{H_2}$ | $i_{as}$ (A/cm$^2$) | $D_{H_2}$ (cm$^2$/s) (cal.) | $D_{H_2,eff}$ (cm$^2$/s) (exp.) | Porosity (%) (exp.) | Tortuosity |
|---|---|---|---|---|---|
| 0.2 | 1.3 | 4.58 | 0.506 | 54 | 4.89 |
| 0.34 | 2.1 | 4.58 | 0.470 | 54 | 5.26 |
| 0.5 | 3.25 | 4.58 | 0.506 | 54 | 4.89 |

**CO-$CO_2$ Binary System**

| $p_{CO}$ | $i_{as}$ (A/cm$^2$) | $D_{CO}$ (cm$^2$/s) (cal.) | $D_{CO,eff}$ (cm$^2$/s) (exp.) | Porosity (%) (exp.) | Tortuosity |
|---|---|---|---|---|---|
| 0.18 | 0.21 | 0.958 | 0.063 | 54 | 8.27 |
| 0.23 | 0.31 | 0.958 | 0.073 | 54 | 7.08 |
| 0.32 | 0.49 | 0.958 | 0.084 | 54 | 6.17 |
| 0.44 | 0.73 | 0.958 | 0.091 | 54 | 5.65 |

**$H_2$-He-$H_2O$ Ternary System**

| $p_{He}$ | $i_{as}$ (A/cm$^2$) | $D_{H_2}$ (cm$^2$/s) (cal.) | $D_{H_2,eff}$ (cm$^2$/s) (exp.) | Porosity (%) (exp.) | Tortuosity |
|---|---|---|---|---|---|
| 0.78 | 1.5 | 5.677 | 0.545 | 54 | 5.62 |
| 0.65 | 2.4 | 5.458 | 0.550 | 54 | 5.35 |
| 0.53 | 3.25 | 5.269 | 0.558 | 54 | 5.10 |
| 0.42 | 4 | 5.108 | 0.556 | 54 | 4.96 |

**$H_2$-$N_2$-$H_2O$ Ternary System**

| $p_{N_2}$ | $i_{as}$ (A/cm$^2$) | $D_{H_2}$ (cm$^2$/s) (cal.) | $D_{H_2,eff}$ (cm$^2$/s) (exp.) | Porosity (%) (exp.) | Tortuosity |
|---|---|---|---|---|---|
| 0.8 | 0.89 | 4.135 | 0.295 | 54 | 7.56 |
| 0.67 | 1.56 | 4.2 | 0.320 | 54 | 7.09 |
| 0.57 | 2.3 | 4.252 | 0.379 | 54 | 6.05 |
| 0.5 | 2.65 | 4.289 | 0.375 | 54 | 6.18 |

**$H_2$-$CO_2$-$H_2O$ Ternary System**

| $p_{CO_2}$ | $i_{as}$ (A/cm$^2$) | $D_{H_2}$ (cm$^2$/s) (cal.) | $D_{H_2,eff}$ (cm$^2$/s) (exp.) | Porosity (%) (exp.) | Tortuosity |
|---|---|---|---|---|---|
| 0.81 | 0.7 | 3.858 | 0.230 | 54 | 9.00 |
| 0.68 | 1.43 | 3.957 | 0.296 | 54 | 7.20 |
| 0.6 | 1.88 | 4.021 | 0.317 | 54 | 6.84 |
| 0.5 | 2.4 | 4.103 | 0.327 | 54 | 6.77 |

vation polarizations and cathodic concentration polarization. The cathodic polarization (activation+concentration) is the same for the two curves. For the test with $H_2$-$H_2O$ as the fuel, at 0.25 A/cm$^2$ the difference between the measured and the calculated polarization (Eq. 33) is ~0.017 V, which includes: (a) cathodic concentration polarization, (b) cathodic activation polarization, and (c) anodic activation polarization. At the same current density, the difference between the measured and calculated polarization (Eq. 34) is ~0.19 V for CO-$CO_2$ as the fuel. However, the cathodic polarizations for (a) and (b) are identical for the two tests. Clearly, greater polarization with the CO-$CO_2$ mixture, beyond what can be attributed to anodic concentration polarization, is attributed to anodic activation polarization. That is, anodic activation polarization with CO-$CO_2$ gaseous mixture of the chosen composition at 0.25 A/cm$^2$ is ~0.173 V higher than that with $H_2$-$H_2O$ gaseous mixture. This also suggests that Ni+YSZ is not a very good anode for CO as the fuel. Indeed, it has been reported in the literature that the electrochemical reaction rate of CO is slower than that of $H_2$ by at least a factor of two.[12] Comparison of performance curves for $H_2$-$H_2O$ mixtures with CO-$CO_2$ mixtures from Fig. 5 and 6 shows that the lower performance with CO-$CO_2$ mixtures cannot be attributed entirely to concentration polarization. Thus, although CO does not poison SOFC anodes unlike PEM fuel cells, its low electrochemical activity, at least with nickel-based anodes, and high concentration polarization suggests that it is not an ideal fuel for SOFCs if a high power density is a requirement.

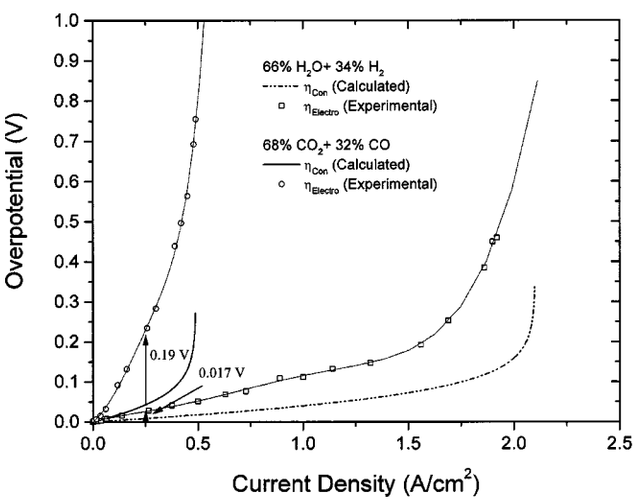


**Figure 12.** Comparison of the measured total polarization (less the ohmic contribution) as a function of current density *vs.* calculated concentration polarization for: (a) ~34% $H_2$ + ~ 66% $H_2O$ and (b) ~32% CO+~68% $CO_2$.

The estimated $D_{H_2}$ using the Chapman-Enskog model and the analysis of multicomponent transport as a function of diluent type and concentration is given in Table II. The experimentally determined $D_{H_2,eff}$ from the anode-limiting current behavior via Eq. 32, which includes the effects of porosity and tortuosity, are also given in Table II. Note that for He as a diluent, the estimated $D_{H_2}$ is higher

than with $N_2$ as the diluent. Table II also shows that estimated $D_{H_2,eff}$ is also similarly higher for He as a diluent compared to $N_2$ as a diluent. Similar trends are observed for $CO_2$ as a diluent. Finally, for CO-$CO_2$ mixtures, the estimated $D_{CO}$ is much lower and so is the $D_{CO,eff}$. In the case of either $N_2$ or $CO_2$ as a diluent, it is also seen that the trends in $D_{H_2}$ and $D_{H_2,eff}$ as a function of composition are similar. That is, the results indicate that except for He, $H_2$ diluted with either $N_2$ or $CO_2$ not only lowers the partial pressure of $H_2$ but also reduces the effective $H_2$ diffusion coefficient. Thus, the diluent can lower cell performance in two ways, reduced $p_{H_2}$ and reduced transport kinetics. From the experimental results (Fig. 3), at 32% $N_2$ dilution the maximum power density was reduced by more than 30%. It was even worse for $CO_2$ dilution with almost 40% reduction of the maximum power density (Fig. 4) at the same diluent concentration. This suggests when either partial oxidation or auto-thermal reforming is used for processing fuel, nitrogen introduced into fuel leads to a lowering of diffusive transport, in addition to fuel dilution. The present work also shows that if in a reforming stage most of the CO is converted to $CO_2$ via a gas shift reaction, in addition to fuel dilution there is also an adverse effect on diffusive transport.

Using $D_{H_2}$, $D_{H_2,eff}$, $D_{CO}$, and $D_{CO,eff}$ and the measured porosity of 54% for the Ni-YSZ anode, the tortuosity factor of the anode, $\tau$, was calculated from Eq. 18 and 19. All of the tortuosity factors fall between 5.0 and 7.0 from $H_2$-$H_2O$ and CO-$CO_2$ binary system measurements (with the exception of one value which is over 8.0) and from $H_2$-$H_2O$ with He, $N_2$ and $CO_2$ dilution (with the exception of one value which is 9). The observation that tortuosity factor is on the order of ~5 to ~7 justifies the use of effective diffusivities. At the same time, the observation that the estimated tortuosity factor does exhibit some variability suggests that it may include effects in addition to purely geometric factors (such as, possibly, adsorption and surface diffusion). A value of five measured by a different method for a Ni-YSZ anode has been reported in the literature.[11] This suggests that the possible effects of adsorption/desorption and surface diffusion must be small in anodes of the present study.

*Cell performance with* $H_2$ + CO *mixture as the fuel*.—The cell performance with as-received CO as fuel was poor because of slow diffusion and slow electrochemical reaction rate, as discussed earlier. However, the cell performance on $H_2$ + CO even when CO concentration was as high as 55% was very high, close to that with as-received $H_2$ (Fig. 8) and quite high with CO content as high as 80%. The diffusion coefficient of $H_2$ in $H_2$-$H_2O$-CO ternary mixtures (ignoring the effects of $CO_2$) may be given by

$$D_{H_2} = \left( \frac{1}{D_{K,H_2}} + \frac{X_{CO}}{D_{H_2,CO}} + \frac{1 - X_{CO}}{D_{H_2,H_2O}} \right)^{-1} \qquad [35]$$

The calculated $D_{H_2}$ ranges between 4.17 and 4.31 $cm^2/s$ for CO mole fraction between 0.8 and 0.5, which is similar to that for $H_2$-$H_2O$-$N_2$. However, the observed performance with $H_2$-CO is much superior to that with $H_2$-$H_2O$-$N_2$ mixtures as the fuel. This is consistent with expectations because a shift reaction is expected in $H_2$-CO gas mixtures during cell operation. At 800°C the standard Gibbs free energy for the gas shift reaction

$$CO + H_2O \Leftrightarrow CO_2 + H_2$$

is only −0.368 kJ/mol.[15] However, the reaction rate constant is very high as reported in the literature and thus it may be assumed that the shift reaction at the anode/electrolyte interface is at equilibrium.[11] Thus, for a fuel gas composition containing greater than 50% $H_2$ (and balance CO), it can be argued that $H_2O$ produced by the electrochemical oxidation of $H_2$ is more than sufficient to react with CO present to form $H_2$ and $CO_2$. In such a case, there should be little difference in performance when compared to pure $H_2$ as fuel (with the exception of a small difference related to differences in concentration polarization). There is very little difference in performance with fuels ranging in composition from ~100% $H_2$ and ~45% $H_2$ + ~ 55% CO, as seen in Fig. 8. For compositions of fuel containing substantially greater than 50% CO, the $H_2O$ produced by the electrochemical oxidation of $H_2$ is not sufficient to shift most of the CO to $CO_2$. The remaining CO has to be oxidized electrochemically to $CO_2$, for which polarization is observed to be much greater (Fig. 6). Indeed, Fig. 8 shows that the performance is much worse with fuels containing ~68% CO+~32% $H_2$ and ~80% CO+~20% $H_2$.

## Conclusions

Based on the present work, the following conclusions are drawn:

1. Anode-supported SOFCs exhibit substantial effect of an inert gas diluent in the fuel on concentration polarization, consistent with expectations based on multicomponent gas diffusion in porous bodies. Specifically, anodic concentration polarization is lower with an inert gas diluent of low molecular weight (such as He) than an inert gas diluent of higher molecular weight (such as $N_2$).

2. For a sufficiently high concentration of the diluent, the voltage *vs.* current density traces exhibits anode limiting current density behavior, characterizing a rapid drop of voltage at a critical current density. This current density was used to estimate the corresponding effective diffusivities.

3. Electrochemical performance with CO + $CO_2$ gas mixtures is much worse than fuel gas mixtures containing $H_2$. This is rationalized in part on higher anodic concentration polarization and slower electrochemical oxidation of CO. The results show that Ni +YSZ is an excellent anode for $H_2$-containing fuel, but not for CO.

4. Studies on cell performance with CO + $H_2$ gas mixtures as fuel show that water gas shift reaction plays a major role. Effectively, as long as the $H_2$ content is greater than ~50%, high performance is maintained by producing additional $H_2$ through the shift reaction. As a result, the cell performance with essentially pure $H_2$ is about the same as that with a $H_2$ + CO gaseous mixture as fuel, as long as the CO concentration is not too high.

## Acknowledgments

This work was supported by the U.S. Department of Energy (NETL) under contract no. DE-AC26-99FT40713.

*The University of Utah assisted in meeting the publication costs of this article.*

## List of Symbols

| | |
|---|---|
| $A$ | cathode area, $cm^2$ |
| $D_i$ | diffusion coefficient of gaseous species i, $cm^2/s$ |
| $D_{K,i}$ | knudsen diffusion coefficient of gaseous species i, $cm^2/s$ |
| $D_{i,eff}$ | effective diffusion coefficient of gaseous species i, $cm^2/s$ |
| $D_{ij}$ | binary diffusion coefficient of gaseous species i and j, $cm^2/s$ |
| $D_{ij,eff}$ | binary effective diffusion coefficient of gaseous species i and j, $cm^2/s$ |
| $E$ | nernst voltage, V |
| $F$ | faraday constant, C/mol |
| $\Delta G°$ | standard free energy change, kJ/mol |
| $i$ | current density, $A/cm^2$ |
| $i_{as}$ | anode-limiting current density, $A/cm^2$ |
| $l_a$ | anode thickness, cm |
| $M_i$ | molecular weight of gaseous species i, g |
| $m_T$ | total molar flow rate of fuel, mol/s |
| $N_i$ | molar flux of gaseous species i, $mol/cm^2$ s |
| $p_i$ | partial pressure of gaseous species i, atm |
| $R$ | ideal gas constant, J/mol K |
| $T$ | temperature, K |
| $V_v$ | volume fraction porosity |
| $W$ | mass, g |
| $x$ | coordinate along the diffusion direction, cm |
| $X_i$ | mole fraction of gaseous species i |

Greek

| | |
|---|---|
| $\eta$ | polarization, V |
| $\sigma_{ij}$ | average collision diameter of gaseous species i and j, A |
| $\tau$ | tortuosity factor |
| $\Omega$ | collision integral |

## References


1. S. DeSouza, S. J. Visco, and L. C. DeJonghe, *Solid State Ionics*, **98**, 57 (1997).
2. J. W. Kim, A. V. Virkar, K.-Z. Fung, K. Metha, and S. C. Singhal, *J. Electrochem. Soc.*, **146**, 69 (1999).
3. T. Tsai and S. A. Barnett, *Solid State Ionics*, **98**, 191 (1997).
4. Y. Jiang and A. V. Virkar, in *Ionic and Mixed Conducting Ceramics (IV)*, T. A. Ramanarayan, Editor, PV 2001-28, p. 374, The Electrochemical Society Proceedings Series, Pennington, NJ (2001).
5. E. P. Murray, T. Tsai, and S. A. Barnett, *Nature (London)*, **400**, 649 (1999).
6. S. Park, R. Cracium, J. M. Vohs, and R. J. Gorte, *J. Electrochem. Soc.*, **146**, 3603 (1999).
7. Y. Jiang and A. V. Virkar, *J. Electrochem. Soc.*, **148**, A701 (2001).
8. R. Peters, E. Riensche, and P. Cremer, *J. Power Sources*, **86**, 432 (2000).
9. E. A. Mason and A. P. Malinauskas, *Gas Transport in Porous Media: The Dusty Gas Model*, Elsevier, Amsterdam (1983).
10. R. R. Remick and C. J. Geankoplis, *Chem. Eng. Sci.*, **29**, 1447 (1974).
11. W. Lehnert, J. Meusinger, and F. Thom, *J. Power Sources*, **87**, 57 (2000).
12. H. Yakabe, M. Hishinuma, M. Uratani, Y. Matsuzaki, and I. Yasuda, *J. Power Sources*, **86**, 423 (2000).
13. Y. Jiang, A. V. Virkar, and F. Zhao, *J. Electrochem. Soc.*, **148**, A1091 (2001).
14. E. E. Underwood, *Quantitative Stereology*, Addison-Wesley, Reading, MA (1969).
15. D. R. Lide and H. V. Kehiaian, *CRC Handbook of Thermophysical and Thermochemical Data*, CRC Press, Inc., Boca Raton, FL (1994).
16. E. L. Cussler, *Diffusion-Mass Transfer in Fluid Systems*, Cambridge University Press, Cambridge, MA (1984).
17. S. Weissman and E. A. Mason, *J. Phys. Chem.*, **37**, 1289 (1962).
18. N. B. Vargaftik, *Handbook of Physical Properties of Liquids and Gases*, 2nd ed., Hemisphere Publication Corporation, Bristol, PA (1976).